Effect of hydrodynamic interaction on partially stretched polymers

Anirban Sain
Physics Department, Indian Institute of Technology–Bombay, Powai, Mumbai 400076, India
(Received 30 October 2007; revised manuscript received 20 May 2008; published 23 June 2008)

We compute the effect of hydrodynamic interaction and stretching on the fluctuation properties of a polymer, with its end points held fixed. Computing the preaveraged hydrodynamic tensor exactly for this geometry, we study both flexible and semiflexible polymer chains, such as Zimm, freely jointed chain, and wormlike chain (WLC) models. We compare the spectra of relaxation-time scales for the effective normal modes of these models. The spectra differ across models with respect to the degree of stretch, but their power-law scaling with low mode numbers turns out to be the same. The characteristics of the transverse modes of WLC agree very well with the experimental data on DNA. The crossover scaling function for $\langle 1/r \rangle$, the inverse of the distance along the polymer contour, yields a modified formula for the size of a "Pincus blob," appropriate for the fixed-end boundary condition.

DOI: 10.1103/PhysRevE.77.061919 PACS number(s): 87.15.H−, 87.16.Ka, 36.20.Ey, 82.35.Pq

Partially extended biopolymers, suspended in fluid, are widely used for single-molecule micromechanical experiments. DNA and various proteins have been studied for their interesting macromolecular elasticity [1,2]. Partially stretched DNA has been used as a template for studying protein-DNA interaction [3]. DNA has also been used for understanding basic polymer dynamics issues, such as vibration properties of stiff polymer chains [4,5] and the influence of shear flow on its conformational dynamics [6]. To stretch the polymer, different means have been used in different experiments, which amounts to different boundary conditions for the equation of motion (EOM). In some studies, one end of the polymer is immobilized, either by sticking it to a wall or by an optical trap, and the polymer is stretched by simply pulling its other end, or subjecting the whole polymer to a flow [6].

Here we study the vibrational modes of a stretched polymer with both of its ends fixed. The polymer has contour length L_0, with its two ends fixed at origin and $(0,0,L)$, respectively. The polymer can be described by a space curve $\mathbf{R}(s)$, where $s \in [0,L_0]$ runs along the contour. Chu *et al.* [5] have shown that stretched DNA, despite being a semiflexible polymer, shows Rouse-like normal modes with relaxation times scaling as $\tau_p \sim p^{-1.7}$ for the long-wavelength modes. Winkler has devised a theoretical formalism for computing the τ_p of semiflexible chains [7]. This theory is based on the maximum entropy principle, which is at best a hypothesis. Dynamical constraints, such as (a) constant bond length $u(s)^2=1$ and (b) fixed end-to-end distance $\mathbf{R}(L_0)-\mathbf{R}(0)=(0,0,L)$, have been converted to statistical constraints, i.e., they are recovered only after averaging over equilibrium fluctuations. These have enabled linearization of the equation of motion, which is otherwise nonlinear because of the dynamical constraint $u(s)^2=1$. Linearization results in Gaussian distribution functions for $P[R(s)-R(s')]$, which allowed for analytic computation of τ_p. Further, for quantitative agreement of τ_p with experiments, the force-extension curve of the polymer has also been used. Note that the linearization mentionedabove is different from the preaveraging approximation [8], which is required after hydrodynamic interaction is introduced through the Oseen tensor. We take a simpler route. We start with the simplest bead-spring model of polymers, namely, the Rouse model, but we introduce a stretch-dependent effective spring constant that is obtained from the force-extension curve [1] of the respective polymer, be it Rouse, freely jointed chain (FJC), or wormlike chain (WLC) (for Rouse, the spring constant is independent of stretch). We then introduce hydrodynamic interaction and compute τ_p for the preaveraged EOM. That allows us to treat both flexible (Zimm, FJC) and semiflexible (WLC) chains [9] with the same formalism and reproduce the experimental results on DNA and simulation results on FJC. The exact calculation of the preaveraged hydrodynamic tensor with fixed boundary conditions brings out a qualitatively different result for the size of the Pincus blob [10]. The scaling of the τ_p's of transverse and longitudinal modes also turns out to be different.

In our description, the end-to-end distance of the polymer is given by the relative extension $z=L/L_0$ and is delimited by $L_0>L \gg R_F=b(N+1)^{\nu}$. Here $L_0=(N+1)b$ is the contour length, where b and $N+1$ are the Kuhn length and the number of bonds, respectively. R_F is the Flory radius [11], $\nu=\frac{3}{5}$ being the Flory exponent. Discretizing the chain in terms of beads and springs, with bead positions $\mathbf{R}_m$, the boundary conditions are $\mathbf{R}_0=0$, $\mathbf{R}_{N+1}=L\hat{z}$. In terms of a $3N$-dimensional supervector $\mathbf{R}=(\mathbf{R_1},\mathbf{R_2},\ldots,\mathbf{R_N})$, the EOM is given by

$$\dot{\mathbf{R}} = H(C\mathbf{R}+\mathbf{f}). \tag{1}$$

$\mathbf{f}$ represents spatially and temporally uncorrelated white noise of thermal orgin. The $(3N\times 3N)$-dimensional matrix C, representing the connectivity of the chain, is given by $C_{nn}=-2k, C_{n,n+1}=C_{n+1,n}=k$ for $n=1,2,\ldots,3N-1$ and $C_{3N,3N}=-2k$, where k is the spring constant.

H is the $(3N\times 3N)$-dimensional Oseen tensor approximating the hydrodynamic interaction [9] among the beads of the polymer and is given by

$$H_{ij}(m,n) = \frac{1}{8\pi\eta_s r}(\delta_{ij}+r_i r_j/r^2),$$

$$H(n,n) = \frac{\mathbf{I}}{\zeta}, \quad \text{where } \mathbf{r} = \mathbf{R}_m - \mathbf{R}_n. \tag{2}$$

$\zeta = 6\pi\eta_s a$ is the Stokes friction on each bead, where η_s and a are the fluid viscosity and the hydrodynamic (Stokes) radius of the bead, respectively. Note that each $H(m,n)$ is a 3×3 matrix.

When the two ends of the chain are fixed, the equilibrium joint distribution $P_{\text{eq}}(\mathbf{R_m},\mathbf{R_n})$, unlike for the free Rouse chain, is no longer a function of $|\mathbf{R_m}-\mathbf{R_n}|$ only. But in terms of the normal-mode amplitudes $\mathbf{X}_p$, the distribution P_{eq} still remains a product distribution $P_{\text{eq}}=\Pi_p P_1(\mathbf{X_p})$. Further, $P_1 \propto \exp(-\frac{1}{2}k_p\mathbf{X_p^2})$, a Gaussian function that is analytically tractable. Hence, no approximations such as the maximum entropy hypothesis [7] are required in order to compute averages.

The static equilibrium configuration of the stretched Rouse chain is $\mathbf{R}_n^{\text{eq}}=(0,0,An)$ [where $A(N+1)=L$]. During vibration, $\mathbf{R}_n=\mathbf{R}_n^{\text{eq}}+\delta\mathbf{R}_n$, where $\delta\mathbf{R}_n$ are the dynamical fluctuations. Note that the EOM of the fluctuations are the same as that of $\mathbf{R}_n$ [Eq. (1)]. These fluctuations satisfy the fixed boundary conditions with nodes at the boundaries. In the absence of hydrodynamic interaction [i.e., $H_{i,j}(m,n) = \delta_{ij}\delta_{mn}/\zeta$], the fluctuations are the sine modes.

The dynamical equation [Eq. (1)] is nonlinear, but the preaveraging approximation, pioneered by Zimm [8], converts these equations into a linear set. In the preaveraging approximation, the H matrix is averaged over the equilibrium distribution, which results in the absence of hydrodynamic interaction, i.e., from the Rouse model. For the Rouse model, the equilibrium probability density $P_{\text{eqlbm}}\propto\exp(-\beta V)$ with the potential energy $V=\frac{1}{2}k\Sigma_n(\mathbf{R}_{n+1}-\mathbf{R}_n)^2$. Diagonalizing this quadratic form in terms of the normal modes, $V\propto\frac{1}{2}\Sigma_p k_p\mathbf{X}_p^2$, where $\mathbf{X}_p$'s are the mode amplitudes defined by

$$\mathbf{R}_n = An\hat{\mathbf{z}} + 2\sum_{p=1}^{N}\mathbf{X}_p\sin(\alpha_p n). \tag{3}$$

The boundary condition fixes $\alpha_p = p\pi/N$. Note that the dynamical equations of the normal modes $\zeta_p\dot{\mathbf{X}}_p = -k_p\frac{\partial V}{\partial \mathbf{X}_p}+\mathbf{f}_p$ [9], where $\zeta_p=2N\zeta$ and $k_p=2Nk\alpha_p^2$, are correctly reproduced by $V(\{\mathbf{X}_p\})$. Also $P_{\text{eq}}\propto\exp(-\beta V)$ yields $\frac{1}{2}k_p\langle\mathbf{X}_p^2\rangle=\frac{3}{2}k_BT$, consistent with equipartition of energy among the decoupled modes at equilibrium.

To compute the preaveraged matrix $H_{ij}(m,n)$, we use its spectral representation [9]

$$\frac{1}{8\pi\eta_s r}\left\langle \delta_{ij}+\frac{r_i r_j}{r^2}\right\rangle = \frac{1}{\eta_s}\left\langle \int_{-\infty}^{\infty}\frac{e^{i\mathbf{q}\cdot\mathbf{r}}}{q^2}\left(\delta_{ij}-\frac{q_iq_j}{q^2}\right)\frac{d^3q}{(2\pi)^3}\right\rangle. \tag{4}$$

Only the $i=j$ components of the matrix (H_{xx},H_{yy},H_{zz}) are nonzero and symmetry of the problem implies $H_{xx}=H_{yy}$. Also the trace $(\Sigma_i H_{ii})$ is given by $(1/2\eta_s\pi)\langle 1/r\rangle = \frac{2}{\eta_s}\int_{-\infty}^{\infty}\frac{1}{q^2}\langle\exp[i\mathbf{q}\cdot\mathbf{r}]\rangle d^3q/(2\pi)^3$.

We substitute $\mathbf{r}=A(n-m)\hat{\mathbf{z}}+\Sigma_p a_p\mathbf{X}_p$, where $a_p = 2[\sin(\alpha_p n)-\sin(\alpha_p m)]$, and then compute $\langle\exp[i\mathbf{q}\cdot\mathbf{r}]\rangle$ by integrating over equilibrium fluctuations of $\mathbf{X}_p$'s,

$$\langle e^{i\mathbf{q}\cdot\mathbf{r}}\rangle = \frac{1}{Z}\int \Pi_p d\mathbf{X_p} e^{-(\beta/2)\Sigma_p k_p\mathbf{X}_p^2 + i\mathbf{q}\cdot[(n-m)\hat{\mathbf{z}}+\Sigma_p a_p\mathbf{X}_p]}, \tag{5}$$

where $Z=\int\Pi_p d\mathbf{X}_p\exp(-\frac{\beta}{2}\Sigma_p k_p\mathbf{X}_p^2)=\Pi_p\sqrt{\frac{2\pi k_BT}{k_p}}$ is the partition function. We first compute $\langle\frac{1}{r}\rangle$ and discuss its various limits. The result for the full hydrodynamic tensor [Eq. (4)] is given later. Integrating over $\{\mathbf{X}_p\}$, we get

$$\left\langle\frac{1}{r}\right\rangle = 4\pi\int_{-\infty}^{\infty}\frac{d^3q}{(2\pi)^3}\frac{1}{q^2}e^{iq_zA(n-m)-(q^2/2)\Sigma_p(a_p^2/k_p)k_BT}$$

$$= 4\pi\int_{-\infty}^{\infty}\frac{d^3q}{(2\pi)^3}\frac{1}{q^2}e^{iqf\cos\theta - q^2G}, \tag{6}$$

where $f=A(m-n)$ and $G(m,n)=\frac{k_BT}{2}\Sigma_{p=1}^{\infty}a_p^2/k_p$.

Before evaluating the integral in Eq. (6), we first verify its free Rouse chain limit. The Rouse chain with free boundary conditions $\partial R_n/\partial n|_{n=0,N}=0$ and $A=0$ (no stretch) leads to $a_p = 2[\cos(p\pi n/N)-\cos(p\pi m/N)]$. Evaluating G, using the identity [9] $\Sigma_{p=1}^{\infty}\frac{1}{p^2}[\cos(p\pi n/N)-\cos(p\pi m/N)]^2=\frac{\pi^2}{2N}|n-m|$, the integral in Eq. (6) reduces to $2\pi\int_0^{\infty}dq\exp(-aq^2)$, where $a=b^2|m-n|/6$. This yields the familiar result $\langle\frac{1}{r}\rangle_{\text{free}} = \frac{1}{b}\sqrt{\frac{6}{\pi}}|n-m|^{-1/2}$.

Returning to the stretched chain, integrating Eq. (6) over θ and q, we obtain

$$\left\langle\frac{1}{r}\right\rangle = \frac{1}{|f|}\,\text{erf}\left(\frac{|f|}{2\sqrt{G}}\right). \tag{7}$$

So both stretching and hydrodynamic interaction influence $\langle r^{-1}\rangle$. The series $G(m,n)$ can be summed up exactly for the stretched chain also, although a_p now involves sine terms: $G(m,n)=\frac{k_BT}{2k}(|m-n|-\frac{(m-n)^2}{N})$. Note that $G(m,n)=G(|m-n|)$ and is symmetric about $|m-n|=N/2$, a reflection of the symmetric boundary condition. To sum the series $G(m,n) = \Sigma_{p=1}^{\infty}g(p)$, we added $g(0)/2=\frac{k_BT}{2kN}(m-n)^2$ to it and converted it to an integral: $\int_0^{\infty}\frac{1}{x^2}[\sin(n\pi x)-\sin(m\pi x)]^2dx=\frac{\pi^2}{2}(|m-n|)$. Note that this addition of the $p=0$ term was not required for the cosine series that appeared in the stretch-free case, since $g(0)=0$ for the cosine series.

We now express Eq. (7) in terms of the relative stretch $z=L/L_o$ and relative interbead distance (along the contour) $x=|m-n|/N$. We also generalize this expression for models of realistic chains with finite extensibility, e.g., the FJC and WLC models. This is done by replacing the spring constant k by k_{eff}, an effective, microscopic spring constant in the expression of G. Experimental force versus longitudinal extension curves [1] for these chains reveals that the macroscopic, effective longitudinal elasticity $k_{\text{eff}}^{(N)\parallel}\equiv F'(L)$ increases steeply at higher relative extensions. Note that we have added the superscript N to distinguish it from the microscopic spring constant of the bonds k_{eff}, which in the effective bead spring models (Rouse or Zimm) scales with the discretization of the macroscopic chain, i.e., $k_{\text{eff}}=Nk_{\text{eff}}^{(N)}$.

Effective elasticity for transverse vibrations is approximately given by $k_{\text{eff}}^{(N)\perp}\equiv F(L)/L$ (this can be shown by perturbing the string at a point in the transverse direction [4,12]). Theoretically such nonlinear force extension curves

$[F(L)]$ have been predicted by considering discrete models of polymers with N bonds with Kuhn length b. Of course $F(L)$ depends on the specific model, namely, FJC [11] or WLC [12,13],

$$F(L) = \frac{2k_BT}{b}\left(\frac{1}{4}(1-z)^{-1} - \frac{1}{4} + z\right) \quad \text{(WLC)}$$

$$= \frac{k_BT}{b}\mathcal{L}^{-1}(z) \quad \text{(FJC)},$$

$$= \frac{3k_BT}{b}z \quad \text{(Rouse/Zimm)}, \tag{8}$$

where the Langevin function $\mathcal{L}(z)=\coth(z)-1/z$. Thus for WLC, $k_{\text{eff}}^{(N)\parallel}=\frac{k_BT}{Nb^2}[2+\frac{1}{(1-z)^3}]$. It is useful to keep in mind that for the WLC model, $b=2l_p$, where l_p is the persistence length. To compute $k_{\text{eff}}^{(N)\parallel}$ for FJC, one needs $\frac{\partial}{\partial L}[\mathcal{L}^{-1}(z)]$. Toward this end, the small and large stretch limits of $\mathcal{L}^{-1}(z)$ are useful. Near $z\to 0$, $\mathcal{L}^{-1}(z)$ has a power-law expansion that yields $F'(L)=\frac{k_BT}{Nb^2}[3+\frac{27}{5}z^2+\frac{297}{35}z^4+\frac{1539}{125}z^6+\cdots]$, while near $z\to 1$, $\mathcal{L}^{-1}(z)=\frac{k_BT}{b}/(1-z)$. These two limits match in the intermediate range $z\in[0.6,0.7]$. The transverse spring constants $k_{\text{eff}}^{(N)\perp}\equiv F(L)/L$ are easier to obtain. In terms of z, x, and k_{eff}, Eq. (7) yields

$$\left\langle \frac{1}{r} \right\rangle = \frac{1}{L_0 z x}\,\text{erf}\left(b\sqrt{\frac{Nk_{\text{eff}}}{2k_BT}}\frac{xz}{\sqrt{x-x^2}}\right). \tag{9}$$

In Fig. 1 we show the behavior of the crossover function. For the Zimm model, the factor $b\sqrt{\frac{k_{\text{eff}}}{k_BT}}=\sqrt{3}$ and in the high stretch limit $(z\to 1)$, $\langle\frac{1}{r}\rangle=\frac{1}{Lx}=\frac{1}{bz|n-m|}$ for $x\to 1$ (since $\text{erf}[\infty]=1$), whereas for $x\to 0$, $\langle\frac{1}{r}\rangle=\frac{1}{b}\sqrt{\frac{6}{\pi}}|n-m|^{-1/2}$ (using $\text{erf}[y]=\frac{2}{\sqrt{\pi}}y$ at small y). The low stretch limit is delimited by $L\sim R_F=b(N+1)^{\nu}$, i.e., $z=L/L_0\to N^{-1+\nu}$. In this limit, Eq. (9) yields $\langle\frac{1}{r}\rangle=\frac{1}{b}\sqrt{\frac{6}{\pi}}|n-m|^{-1/2}$ for $x\to 0$ irrespective of the Flory exponent (ν), whereas for $x\to 1$, $\langle\frac{1}{r}\rangle=\frac{1}{Lx}$. Note that $x\to 1$ refers to a pair of beads near the two fixed boundary points, which are maintained at a distance L. So $\langle\frac{1}{r}\rangle=\frac{1}{Lx}$ is always expected in the $x\to 1$ limit, irrespective of the stretch. The crossover scale x_* at which the scaling changes from $1/\sqrt{x}$ to $1/x$ is obtained by setting the argument of the error function (erf) in Eq. (9) to 1. This yields the size of the "Pincus blob" [10],

$$x_* \sim (1 + zL_0F/k_BT)^{-1}. \tag{10}$$

Qualitatively, as F increases, x_* decreases, but x_* differs quantitatively from the conventional formula $x_*=k_BT/FL_0$ [10], which was derived for a different geometry. They match at high stretch $(z\to 1)$ when zF is large.

Although $\langle 1/r\rangle$ reveals the equilibrium shape of the stretched polymer, calculation of the relaxation times (τ_p) of the normal modes (which are no longer sine modes in the presence of the hydrodynamic interaction) requires the evaluation of the full hydrodynamic tensor [Eq. (4)]. Since the hydrodynamic matrix has a block-diagonal structure, the equations of motion for R_z and R_x (or R_y) get decoupled. As

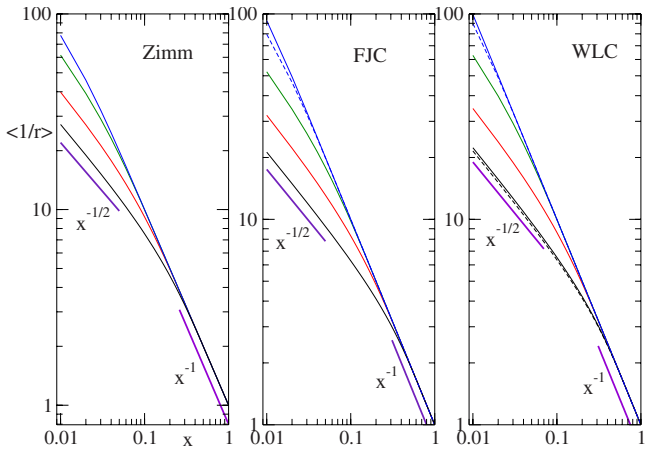

FIG. 1. (Color online) Scaled plots of $\langle 1/r\rangle$ versus x $(=|n-m|/N)$ for the Zimm, FJC, and WLC models for different relative stretches (z). Chain parameters $N=100$, $b=1$, and $a=0.1$ are the same for all the models. Curves, from top to bottom, are for $z=0.8,0.5,0.3,0.2$ (while $z_{\min}=N^{-2/5}=1.585$). Data at large x have been collapsed by dividing the y axis by $1/L_0z$, which is the maximum value for $\langle r^{-1}\rangle$. The asymptotic scaling regimes (random walk scaling $1/\sqrt{x}$ at short distance and $1/x$ scaling at long distance) are indicated. Here we have used the value of k_{eff} corresponding to the longitudinal vibration modes. Using the value for the transverse modes does not change the graphs significantly (shown by dashed lines).

a result, $\dot{R}_z$ and $\dot{R}_x$ involve only H_{zz} and H_{xx}, respectively. The eigenvalues of these two EOMs lead to the τ_p's of the longitudinal and transverse modes. The expressions for H_{xx} and H_{zz} can be computed analytically,

$$H_{zz} = \frac{1}{8\pi\eta_s f}\left[\left(1-\frac{1}{2y^2}\right)\text{erf}[y] + \frac{1}{y}e^{-y^2}\right],$$

$$2H_{xx} = \frac{1}{8\pi\eta_s f}\left[\left(3+\frac{1}{2y^2}\right)\text{erf}[y] - \frac{1}{y}e^{-y^2}\right], \tag{11}$$

where $y=|f|/2\sqrt{G}$. Using this tensor, we numerically compute the eigenspectrum $\{\lambda_p\}$ of the HC matrix [Eq. (1)] and get $\tau_p=1/\lambda_p$. It is well known [14] that the Oseen tensor has singularities at moderate values of $\lambda=\zeta/8\pi\eta_s b$. With Stokes coefficient $\zeta=6\pi\eta_s a$ and assuming that the beads of the bead-link chain are just touching each other, $\lambda_{\max}=\frac{3}{8}$. It has been argued that actual values of λ in a bead-link picture of the DNA [15] are 0.1354. We chose $\lambda=0.1$ for our numerical evaluation and checked that for $\lambda=0.05$ the τ_p's do not change significantly. But for $\lambda=\frac{3}{8}$ the effects of the singularity are felt and the eigenvalues of the HC matrix become negative for large p's. The effect of the singularities is often missed out in analytic approximations [7] for τ_p.

Note that the difference among the Zimm, FJC, and WLC models (Fig. 1) emerges from their difference in k_{eff}. For the Zimm model, k_{eff} is constant, while for FJC and WLC it increases with z, and more steeply for WLC. The length scale b in the expressions for k_{eff} [Eq. (8)] is the Kuhn length of the respective polymer models. For WLC, the Kuhn length $b=2l_p$, where l_p is the persistence length. The experimental

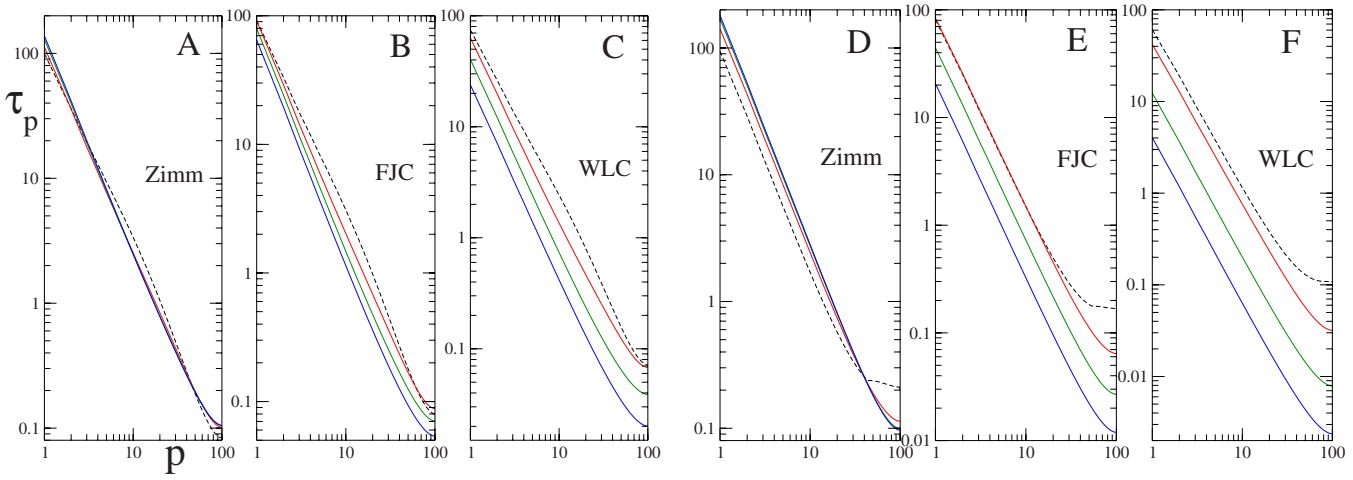

FIG. 2. (Color online) τ_p (in units of $6\pi\eta_s ab^2/k_BT$) versus p for the transverse modes (A), (B), (C) and longitudinal modes (E), (F), (G) for the Zimm, FJC, and WLC models for different z values (=0.5, 0.7, 0.8 from top to bottom). The spectra for $z=0.3$ are shown separately by a dotted line. For the Zimm model, the spectra for $z>0.3$ are almost indistinguishable from each other. Chain parameters are $N=100$, $b=1$, and $a=0.1$.

data on DNA, to which we will compare our theoretical spectrum, were obtained with DNA strands of contour length 20 μm, much larger than its persistence length 53 nm. We mimic this situation by choosing $N=100$ and $b=1$ such that $L_0=Nb \gg l_p$.

Figure 2 shows the τ_p spectrum for both transverse and longitudinal modes for the different models. Power-law scaling $\tau_p \sim p^{-n(z)}$ is visible up to $p \leq 30$. The exponent $n(z)$ changes with relative stretch z. As is clear from Fig. 3, $n(z)$ differs between longitudinal and transverse modes, but is not significantly different across models. The exponents of the transverse modes agree very well with experimental data on DNA in Ref. [5]; in particular, at high stretch the scaling exponents are close to -1.7. In the experimental data, as z is varied from $z=0.3$ to 0.8, the slowest time scale τ_1 is reduced, approximately, by three times, which is also reproduced by our theory. Longitudinal exponents have not yet been reported experimentally; they are much more difficult to measure. The main difference among the models is their sensitivity to stretch: as z is changed, τ_p varies across a wider range of values as we go from the Zimm to the FJC to the WLC model. Also this variation is relatively higher for the longitudinal modes compared to the transverse ones. These may be traced back to a steeper rise in k_{eff} as z increases, for finitely extensible models, and the fact that for WLC it is steeper than that of FJC. Also k_{eff} is steeper for the longitudinal modes compared to the transverse modes. De Gennes had argued [16] that at high stretch, hydrodynamic interaction should become very weak and hence the Rouse exponent $\tau_p \sim p^{-2}$ should be recovered as $z \to 1$. Our data show that this is not true, at least for "fixed" boundaries. Also note that at high stretch, the scaling exponents of the FJC and WLC models are indistinguishable. This is because at such high stretch there is hardly any bending (which otherwise distinguishes WLC from FJC).

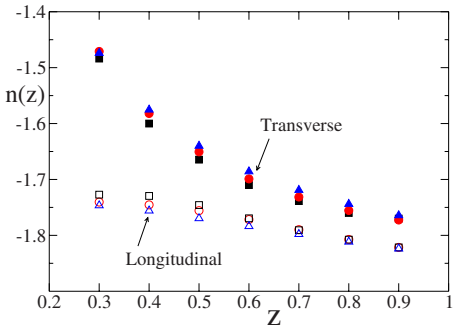

FIG. 3. (Color online) Scaling exponent for the spectrum of relaxation times (for the $p<13$ modes) versus relative stretch z, for Zimm (triangles), FJC (circles), and WLC (squares). The slopes are extracted from graphs as in Fig. 2.

In Fig. 4, we plot the slowest relaxation time scale τ_1 versus stretch. It is qualitatively different for infinitely extensible (Zimm) and finitely extensible (FJC, WLC) models. For the FJC and WLC models, (a) transverse modes are slower (i.e., higher τ_1) compared to the longitudinal ones, and (b) τ_1

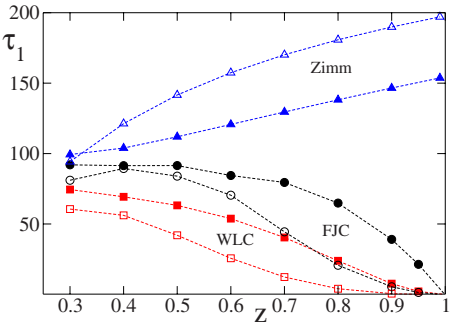

FIG. 4. (Color online) Slowest relaxation time τ_1 versus relative stretch z for the transverse (filled symbols) and longitudinal (open symbols) modes for different models: Zimm (triangles), FJC (circles), and WLC (squares). The symbols are joined by dashed lines to guide the eye. The relaxation times are given in units of $6\pi\eta_s ab^2/k_BT$, using the same chain parameters: $N=100$, $b=1$, and $a=0.1$ for all the models, except k_{eff}, which distinguishes the models.

decreases at higher stretch. For the Zimm model, the trends are just the opposite and the difference between the longitudinal and transverse modes arises due to the difference in H_{zz} and H_{xx}, while k_{eff} is the same for them. Thus the purely hydrodynamic effect slows down the longitudinal modes with respect to the transverse ones, whereas stretch-dependent nonlinear elasticity has the opposite effect and is relatively stronger than the hydrodynamic effect as seen for FJC and WLC. For FJC, our data on τ_1 agree with the numerical simulation of [12]. For WLC also Ref. [12] gives a theoretical plot of τ_1 versus stretch. The qualitative difference between the plots is that, at low stretch, τ_1 for FJC is rather flat and it varies steeply at high stretch, while for WLC the variation is rather uniform with stretch. Our data reproduce all these trends. However, note the difference in the scale of τ_1 between FJC and WLC in their plots. One of the reasons for this is the difference in the number of bonds (N). τ_1 typically increases with N (e.g., for the Rouse chain $\tau_1 \propto N^2$). In Ref. [12], for FJC the authors chose $N=20$, $b=50$ nm, and $a=10$ nm, while for WLC, $N=20\ \mu\mathrm{m}/b \sim 200$. We have $N=100/b=100$ and $a/b=0.1$ for all our graphs.

In summary, we have computed the relaxation spectrum of both finite and infinitely extensible polymers by an exact treatment of the preaveraged hydrodynamic tensor (obeying the correct boundary conditions) and incorporating the stretch-dependent, nonlinear, macroscopic elasticity of the polymer. It may be possible to experimentally verify our predictions for the FJC model using alkane chains. To verify our predictions for the longitudinal modes, at least the long-wavelength ones, attaching fluorescent markers on the chain at regular intervals may be useful.

Support from a Seed grant-IIT Bombay, India is acknowledged.

[1] S. B. Smith, L. Finzi, and C. Bustamante, Science **258**, 1122 (1992).
[2] M. S. Z. Kellermayer, S. B. Smith, H. L. Granzier, and C. Bustamante, Science **276**, 1112 (1997).
[3] Y. M Wang, R. H. Austin, and E. C. Cox, Phys. Rev. Lett. **97**, 048302 (2006).
[4] J.-C. Meiners and S. R. Quake, Phys. Rev. Lett. **84**, 5014 (2000).
[5] S. R. Quake, H. Babcock, and S. Chu, Nature **388**, 151 (1997).
[6] D. E. Smith, H. P. Babcock, and S. Chu, Science **283**, 1724 (1999).
[7] R. G. Winkler, Phys. Rev. Lett. **82**, 1843 (1999).
[8] B. H. Zimm, J. Chem. Phys. **24**, 269 (1956).
[9] M. Doi and S. F. Edwards, *The Theory of Polymers Dynamics* (Clarendon, Oxford, 1986).
[10] P. Pincus, Macromolecules **9**, 386 (1976).
[11] P. J. Flory, *Statistical Mechanics of Chain Molecules* (Hanser, New York, 1989).
[12] J. W. Hatfield and S. R. Quake, Phys. Rev. Lett. **82**, 3548 (1999).
[13] J. F. Marko and E. D. Siggia, Macromolecules **28**, 8759 (1995).
[14] R. Zwanzig, J. Kiefer, and G. H. Weiss, Proc. Natl. Acad. Sci. U.S.A. **60**, 381 (1968).
[15] B. H. Zimm, Macromolecules **31**, 6089 (1998).
[16] P. G. De Gennes, J. Chem. Phys. **60**, 5030 (1974).